



Mapping Titan's surface features within the visible spectrum via Cassini VIMS

Graham Vixie^{a,*}, Jason W. Barnes^a, Jacob Bow^a, Stéphane Le Mouélic^b, Sébastien Rodriguez^c, Robert H. Brown^d, Priscilla Cerroni^e, Federico Tosi^f, Bonnie Buratti^g, Christophe Sotin^g, Gianrico Filacchione^e, Fabrizio Capaccioni^e, Angioletta Coradini^f

^a University of Idaho, Department of Physics, P.O. Box 440903, Moscow, ID 83844-0903, United States

^b Laboratoire de Planétologie et Géodynamique, CNRS UMR 6112, 2 rue de la Houssinière, Université de Nantes, 44300 Nantes, France

^c Laboratoire AIM, Université Paris Diderot - Paris 7/CNRS/CEA-Saclay, DSM/IRFU/SAP, Gif sur Yvette, France

^d University of Arizona, Lunar and Planetary Laboratory, 1629 East University Blvd, Tucson, AZ 85721-0092, United States

^e Istituto di Astrofisica Spaziale e Fisica Cosmica, Sezione di Roma, Via Fosso del Cavaliere 100, Tor Vergata, IT 00133 Roma, Italy

^f Istituto di Fisica dello Spazio Interplanetario, Via Fosso del Cavaliere 100, IT 00133 Roma, Italy

^g California Institute of Technology/Jet Propulsion Laboratory, 4800 Oak Grove Drive, Pasadena, CA 91109, United States

ARTICLE INFO

Article history:

Received 11 September 2010

Received in revised form

25 March 2011

Accepted 29 March 2011

Available online 8 April 2011

Keywords:

Titan

Surface

Optical wavelength

Visible imaging

Cassini VIMS

ABSTRACT

Titan shows its surface through many methane windows in the 1–5 μm region. Windows at shorter wavelengths also exist, polluted by scattering off of atmospheric haze that reduces the surface contrast. At visible wavelengths, the surface of Titan has been observed by Voyager I, the Hubble Space Telescope, and ground-based telescopes. We present here global surface mapping of Titan using the visible wavelength channels from Cassini's Visual and Infrared Mapping Spectrometer (VIMS). We show global maps in each of the VIMS-V channels extending from 0.35 to 1.05 μm . We find methane windows at 0.637, 0.681, 0.754, 0.827, 0.937, and 1.046 μm and apply an RGB color scheme to the 0.754, 0.827 and 0.937 μm windows to search for surface albedo variations. Our results show that Titan appears gray at visible wavelengths; hence scattering albedo is a good approximation of the Bond albedo. Maps of this genre have already been made and published using the infrared channels of VIMS. Ours are the first global maps of Titan shortward of 0.938 μm . We compare the older IR maps to the new VIMS-V maps to constrain surface composition. For instance Tui Regio and Hotei Regio, referred to as 5- μm bright spots in previous papers, do not distinguish themselves at all visible wavelengths. The distinction between the dune areas and the bright albedo spots, however, such as the difference between Xanadu and Senkyo, is easily discernible. We employ an empirically derived algorithm to remove haze layers from Titan, revealing a better look at the surface contrast.

© 2011 Elsevier Ltd. All rights reserved.

1. Introduction

We present here findings from the Cassini spacecraft, which is on its second extended mission, via the Visual and Infrared Mapping Spectrometer (VIMS) instrument (Brown et al., 2004). Most of Titan's surface has already been seen from RADAR and infrared wavelengths, but surface features have been sparsely identified in the visible spectrum. Methane windows do exist in the visible, albeit not as transparently as in the IR; using them, new constraints can be placed on the composition of Titan's surface.

The ability to view Titan's surface was pioneered near the beginning of the 1990s with the discovery of near-infrared methane windows by McKay et al. (1989) and Griffith et al.

(1991). Titan's surface was first seen in optical wavelengths by Voyager I as discussed by Richardson et al. (2004) using wavelengths ranging from 590 to 640 nm, and by Smith et al. (1996) using the window at 0.94 μm . The Hubble Space Telescope (HST) also observed Titan's surface at 673 nm (Smith et al., 1996). Relative brightness maps of Titan were produced from the HST data by Smith et al. (1996) and with Cassini's Imaging Science Subsystem (ISS) by Turtle et al. (2009, 2011).

The VIMS visible channel measures optical spectra from 0.351 to 1.05 μm split up over 96 channels using a slit-scanning visible spectrometer (Capaccioni et al., 1998). We can then peruse each wavelength channel to identify which wavelengths can pierce through Titan's atmosphere to the surface. This has been done in infrared channels by Barnes et al. (2007), but comprehensive global maps have not been previously produced at wavelengths shortward of 0.938 μm . Spectra of Titan in the visible range were published in Neff et al. (1984) and Lockwood et al. (1986) where each paper suggested visible windows. Local maxima in the

* Corresponding author. Tel.: +1 509 6693398.

E-mail address: gvixie@vandals.uidaho.edu (G. Vixie).

spectrum longward of 600nm represent the window wavelengths (although their utility in sensing the surface was not realized at the time), and higher signal-to-noise spectra are presented and discussed by Karkoschka (1994). The work that we describe here is the first to show Titan's surface and monitor some heterogeneities shortward of 0.9 μm .

The goal of this study is to constrain surface composition by generating and analyzing a global map of Titan using methane windows in the optical spectrum. In Section 2 we produce a map using data from five of Cassini's flybys: T8, T9, T31, T34, and rev9. For more information on the observations on these flybys, see Barnes et al. (2009). These flybys were chosen to minimize variance in phase on the global map while maximizing area covered on Titan. We then combine the resulting data together at each wavelength to show surface features on Titan. The end product is a global scale, atmospherically uncorrected, 25-color map. The process of calibrating each individual cube of data and making the maps is outlined in detail in Barnes et al. (2007). The purpose of these maps is to provide another comparative point to the IR maps in hopes of further constraining surface composition and more accurately defining the surface features, which we do in Sections 3–5.

2. Processing of imaging observations

2.1. Mapping

Titan's surface is obscured by scattering and absorption by both haze and methane in the atmosphere in optical wavelengths. At most infrared wavelengths, Titan's atmospheric methane absorbs heavily, making the surface impossible to see. We use Cassini VIMS to scan Titan at all wavelengths to find certain windows where incident solar flux can pass through nearly unhindered and return a signal from the surface. We focus on certain optical wavelength windows where photons are not absorbed the atmosphere.

We start the map making process by selecting all observations where surface features are apparent. Next, we wrote software to place all data cubes from these observations on a single cylindrically projected map based on each cube's embedded latitude and longitude information. We then found certain wavelengths where the surface of Titan becomes apparent by looking at these combined observations at every available wavelength. Fig. 1 shows Titan at all the visible wavelength channels on the VIMS instrument. The three wavelengths showing the most surface features from observation are 0.754, 0.827, and 0.937 μm . The final step was then to create a color composite by assigning each of these wavelengths a color and optimizing contrast in order to show surface variations. We assign the colors blue, green, and red, respectively, to define the RGB map. Fig. 2 shows all identified optical wavelength methane windows at constant contrast. The flybys and individual observations were chosen to maximize longitudinal coverage and be close in phase. Information regarding each flyby used may be found in Table 1. We present then our global scale, atmospherically uncorrected RGB surface reflectivity map of Titan in Fig. 3. This map can then be compared to other known IR maps (see Fig. 4) to identify surface characteristics.

The 0.937 μm reveals the most surface features out of the visible channels since the atmosphere absorbs the least at this wavelength. However, we use two other channels for several reasons. First, we are comparing the surface at different wavelengths and therefore wish to identify any anomaly that is limited to a certain wavelength(s). This is achieved through the creation of the color composite. Features that show more strongly in one (or two) of our primary colors are easier to constrain. Second,

global maps of Titan have already been published in the 0.937 μm wavelength courtesy of ISS. Finally, the more wavelength we can incorporate in to our map while still maintaining surface albedo variability, the greater coverage we have of the spectrum on Titan.

We can identify many familiar landmarks in Fig. 3 such as Shangri-La, Xanadu, and the sideways "H" of Fensal and Aztlan. Five-micron-bright regions like Tui Regio (Barnes et al., 2006) and Hotei Regio (Soderblom et al., 2009; Barnes et al., 2005) do not show strong contrast in the visible map like in the IR maps, as shown in Fig. 4, nor do the Selk or Sinlap craters. These regions are all gray at shorter wavelengths. While the visible color is orange, for clarification, we use the word "gray" to mean that the spectral response is flat and the reflectivity does not vary significantly with wavelength in the visible part of the spectrum.

The global views of Titan (orthographic projections) give an undistorted look at surface features (Fig. 3 bottom). The dark lines that appear on the global maps are seams between the different flybys. The seams are present mostly due to differing phase angles between flybys, limb-darkening, and not being able to fully correct atmospheric effects. The solar incidence and emission angles change over the course of a single flyby as well. Fig. 5 shows the change in these angles and pinpoints the locations of nadir points. At different phase angles, the flyby appears darker, lighter, smoother, or more noisy. The effect of changing phase angles will be discussed in Section 3. Special attention was paid to weaving the different flybys together, as we want the map to look as seamless as possible. The figure of merit used by Barnes et al. (2007) was changed to solely rely on the emission angle in an effort to minimize the seams between flybys.

Noise here is not instrument noise, but rather stripe noise in the VIMS-V instrument. At the end of each row of pixels in the slit scanner, there is a column shielded that measures dark current. The background measured by this dark stripe is actually only measured by a single pixel (the rest of the measurements is thrown away) then subtracted from all the other pixels. The problem here is sometimes a photon will get in and be measured by this pixel giving a higher value to the background. This is also the origin of the striping on the maps. The noise then does not come from the image or the haze, but rather the instrument itself.

Atmospheric scattering is what drives the different appearance as a function of observation geometry. As light from the Sun enters Titan's atmosphere, many possible paths emerge after the light encounters atmospheric haze particles. The light may (ideally) reflect from the surface and go directly to Cassini; more probably, however, the photons collides with haze particles and scatters. This greatly decreases the fraction of photons that successfully travel to Titan's surface and back. Part of this indirect light, backscattered to the spacecraft by Titan's haze without reaching the surface, causes additive offsets that must be corrected (visible – Perry et al., 2005; IR – Rodriguez et al., 2006; Le Mouélic et al., 2008, 2010).

2.2. Haze removal and comparison

Owing to high optical depth, spherical geometry, and uncertainties in scattering properties, it is not presently possible to properly correct for the atmospheric conversion of incident solar flux (I/F) to albedo using radiative transfer. The work of Perry et al. (2005) on ISS data allows us to further our mapping algorithms by empirically compensating for some of the haze to enhance surface contrast. The purpose of this article is present maps, and thus further analysis of atmospheric or haze corrections is beyond the scope of this paper. We did try simple subtraction and ratio based techniques, but our best results came using the ISS techniques directly.

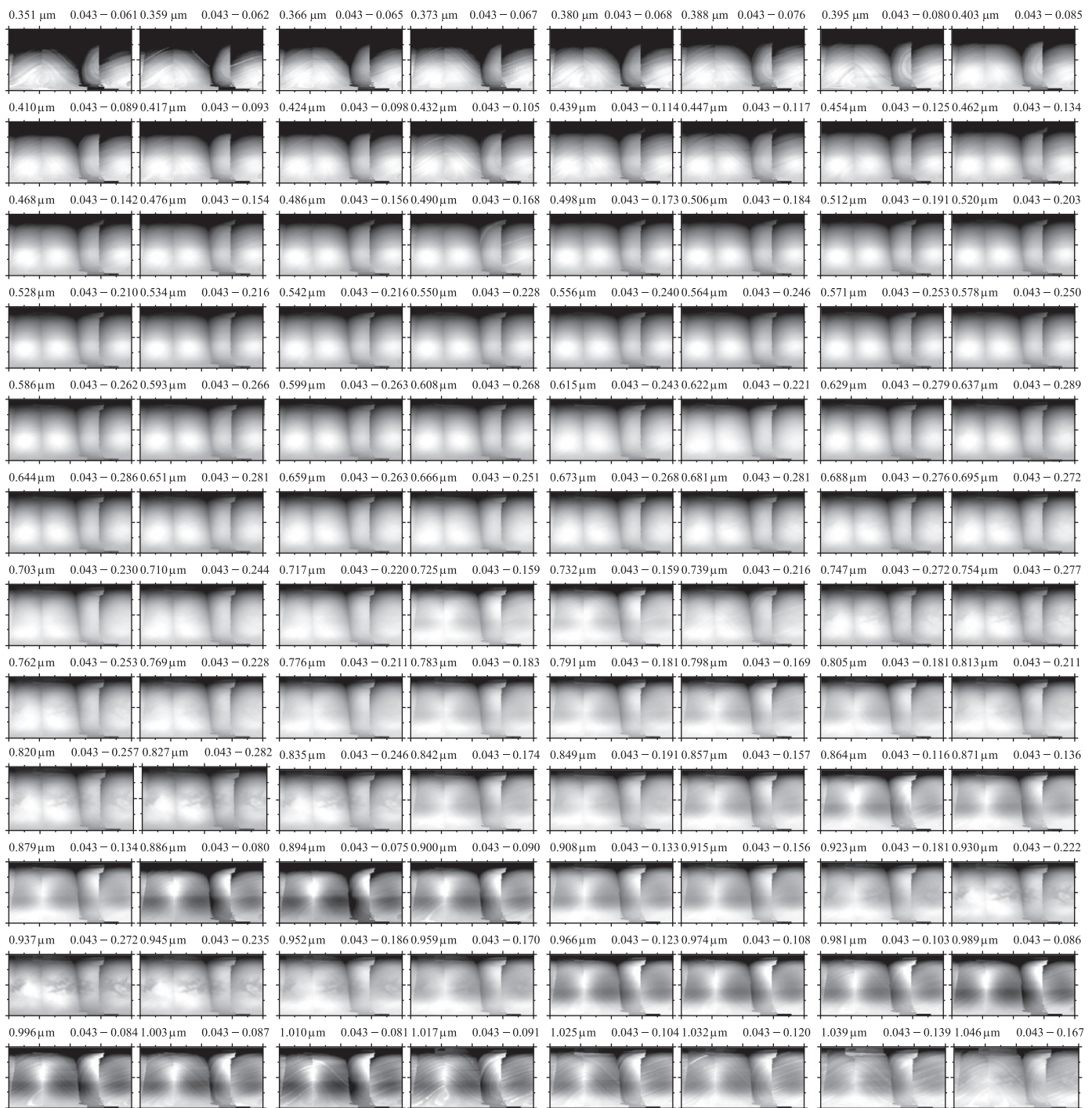


Fig. 1. The top left window represents the beginning of the wavelength range of Cassini VIMS' 96 optical wavelength channels, 0.35 μm , and wavelength increases for each row. A quick look over all of the different wavelengths in the figure above reveal that there are few that show the surface. Methane has fewer windows in the optical spectrum than it does in the infrared, and scattering is more prevalent, but we can still see distinctions on Titan's surface.

Using the I/F maps in Fig. 1 as our starting point, we created a haze-only map using nine wavelengths where our signal is almost completely absorbed and that showed no surface features whatsoever. The wavelengths used to make the haze map are 0.585, 0.599, 0.607, 0.622, 0.651, 0.659, 0.666, 0.709, and 0.878 μm . Following the Perry et al. (2005) algorithm, we divided the original map (Fig. 3) at each of the methane window wavelengths labeled in Fig. 2a by the haze map to create a new, empirically haze-corrected map (Fig. 2b). Using the same color/wavelength setup as the original, we created a new global RGB map (Fig. 6). Trial and error by Perry et al. (2005) shows that a subtraction step

yields lower-quality results. By compensating for wavelengths where our signal is nearly totally absorbed, we make surface features more visible. The resulting map has slightly more striping, but accounts for phase angle as to reduce the visibility of the seams between flybys. Most importantly, the new map shows an improved view of the surface features of Titan as well as reveals some new areas that are barely or not at all visible without correction. Comparing Figs. 3 and 6 show that the dark areas on Titan cover more area with some new areas appearing south of Shangri-La in the west, through the north of Tsegihi, and south of Belet in the east. The improved contrast of the map in

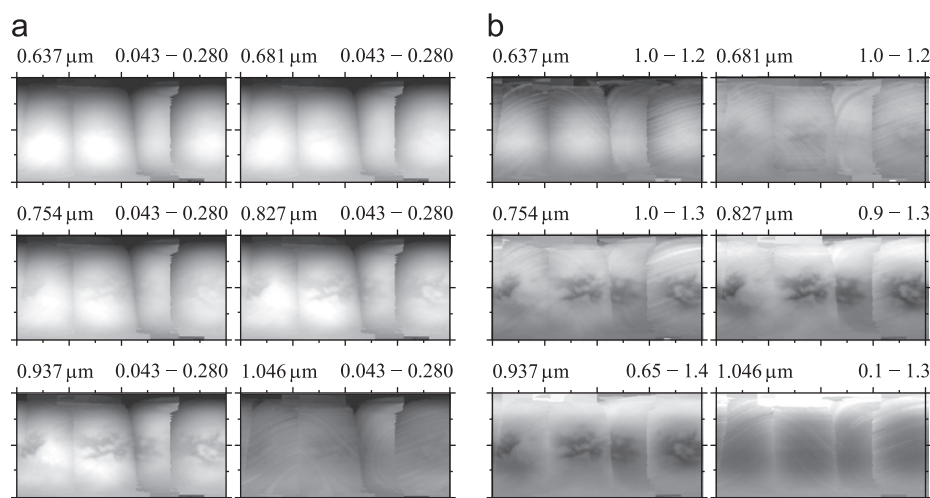


Fig. 2. On the left are I/F maps of Titan without atmospheric correction. Wavelength and contrast are listed in the top left and top right, respectively, of each image. On the right are corrected maps, with the haze divided out according to the Perry et al. (2005) empirical algorithm described in the text. Contrast is constant in the left set of images and set to maximize surface feature distinction in the right.

Table 1

This table summarizes the *Cassini* observations used in this paper.

Flyby	Rev number	Date	Subsolar point	No. of cubes	Phase angle	Best spatial sampling (km)
N/A	rev9	2005 June 6	21.1°S 145°W	6	71°	109
T8	rev17	2005 October 28	19.6°S 139°W	18	21°	42
T9	rev19	2005 December 26	18.9°S 45°W	25	35°	2.9
T31	rev45	2007 May 28	12.0°S 156°E	11	22°	11
T34	rev48	2007 July 19	11.3°S 78°E	8	38°	8
Ta	revA	2004 October 26	23.2°S 165°W	1	9°	2.6
T3	rev3	2005 February 15	22.2°S 155°W	1	20°	7
T10	rev20	2006 January 15	18.7°S 127°W	1	28°	3.9
T12	rev22	2006 March 18	17.9°S 96°W	1	53°	7

Fig. 6 makes the empirically corrected visible maps much more useful than the uncorrected map (Fig. 3).

Stephan et al. (2009) created a global albedo map of Titan using data collected from 2004 to 2008 by the ISS via a narrow band pass filter set at 0.938 μm (Porco et al., 2004). The albedo differences were described in Turtle et al. (2009) as being compositionally related as opposed to topographical. This map was also refined using the same method listed in Perry et al. (2005) and is compared with Fig. 6 in part in Section 4. The color scheme in Fig. 6 helps to distinguish the surface reflectivity differences. As discussed later, there are some areas present in our visible map that are obscured by haze in the ISS 0.938 μm map.

3. Spectroscopy

A spectral comparison between bright and dark surface albedos on Titan's surface tells us how much light at every wavelength channel in the VIMS instrument transmits or is absorbed going through the atmosphere. We choose areas of the same size, one bright and one dark region on Titan near each other so that we have similar phase angle at each location. The regions chosen were from the T8 flyby of Xanadu and Shangri-La and are boxes of uniform albedo along the same latitudinal lines. The longitude for Xanadu's region is from 145°W to 140°W and Shangri-La's is from 155°W to 150°W with the shared latitude region from 8°S to 12°S for a total of 20 pixels per box (Table 1). The plot in Fig. 7 is a spectral ratio dividing Xanadu by Shangri-La. This spectral ratio

shows the precise outlines of methane windows at 0.637, 0.681, 0.754, 0.827, 0.937, and 1.046 μm . A spectrum similar to this was presented in Lemmon et al. (2002) by subtracting a dark area spectrum from a bright area spectrum and the visible methane windows are resolved, albeit with low I/F. Lemmon et al. (2002)'s spectrum anticipates our Fig. 7 which further resolves Titan's visible spectrum and constrains the wavelengths where surface features are visible. Light from Titan's surface may be seen within these wavelengths by any Earth-based telescope sporting Adaptive Optics, given the right filter. Voyager 1 resolved Titan's surface via a slight albedo difference (Richardson et al., 2004), though this was not recognized for 25 years after the flyby.

The phase angle, the angle from Cassini to Titan to the Sun, affects the spectra because of changing haze scattering properties. The spectrum in Fig. 7 was taken from the T8 flyby which had an ingress phase angle of 21°. We compare this T8 spectrum to Tsegihi/Aztlan in Ta, T3, T10, and T12 to sample the effect of phase angle on surface contrast. The dates and phases of each flyby are listed in Table 1. Rannou et al. (2003) did a center-to-limb contrast variation previously at 673 nm by showing a greater relative contrast in bright and dark surface features the further the distance from the limb.

Fig. 8 shows spectra from each flyby alongside each other for comparison. A value of 1 indicates that the regions of Tsegihi and Aztlan look the same at the given wavelength. The trend that we find here is that as phase angle increases, the systematic effects of haze increase and the baseline goes above 1, reducing the effective I/F of transmission peaks (i.e. inhibiting surface viewing).

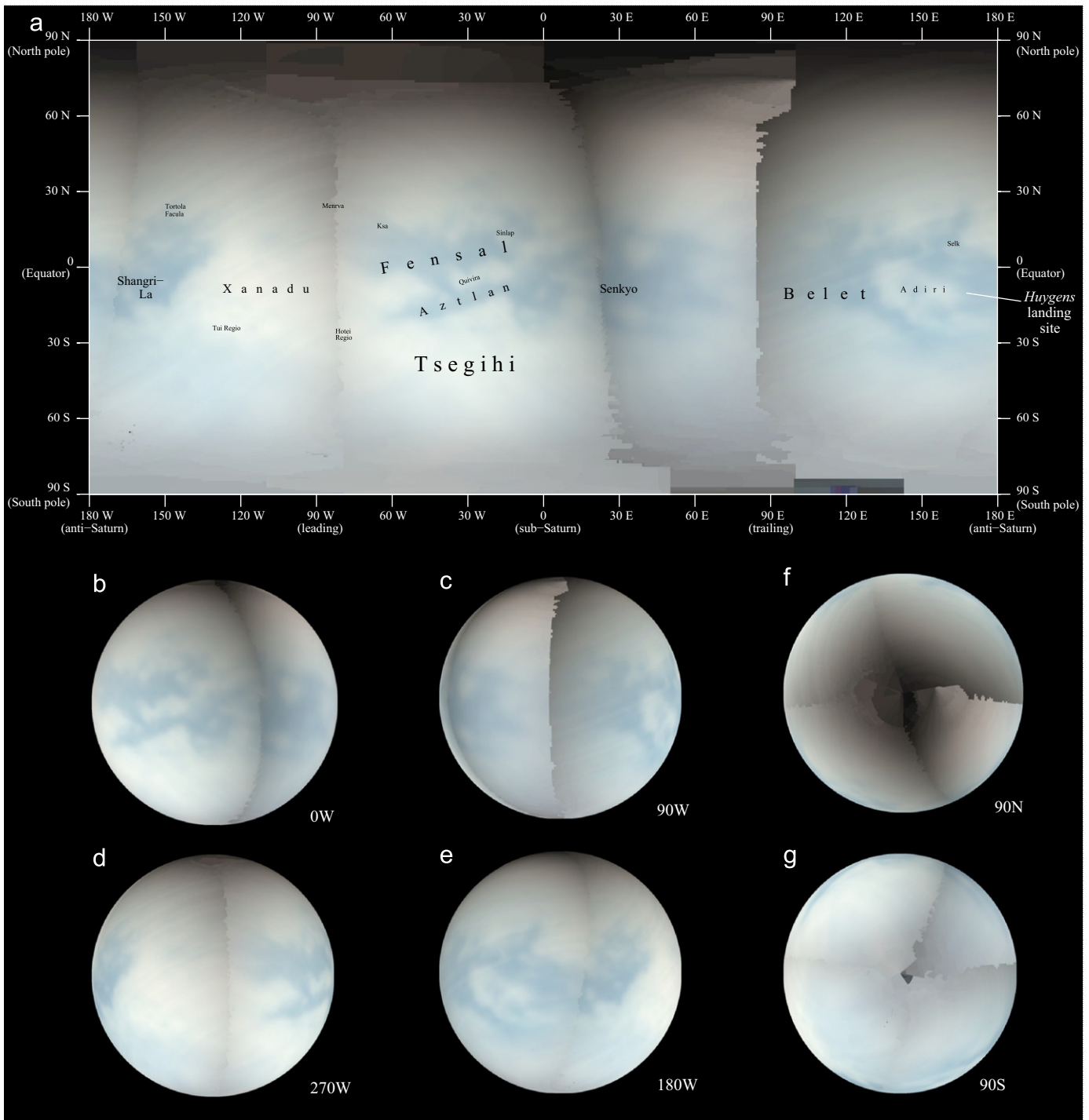


Fig. 3. The atmospherically uncorrected I/F map of Titan shown is made via VIMS from T8, T9, T31, T34, and rev9 in cylindrical projection (a). The colors and wavelengths used to make this map are red at $0.937 \mu\text{m}$, green at $0.827 \mu\text{m}$, and blue at $0.754 \mu\text{m}$. Part a of the figure shows a simple cylindrical map of the five flybys sewn together. Parts b–g of the figure show the different faces of Titan in an orthographical projection. In comparison to infrared maps, our optical map shows less distinction between different wavelengths. However, note that the $5\text{-}\mu\text{m}$ bright spots do not stand out with the exception of Tui Regio. (For interpretation of the references to color in this figure legend, the reader is referred to the web version of this article.)

The height of the intensity peak remains constant above the height of the baseline as phase increases. The spectrum for Ta compared to the spectrum for T12 has the baseline much closer to unity and shows less scattering; this suggests that low phase angles yield clearer results. Judging from the level of noise in the T12 flyby, there seems to be a phase angle at which the data become too noisy to be useful. The lower the phase angle is, the less scattering occurs and the better quality surface viewing is. When the phase angle is high, the lower I/F from limb-darkening

reduces the signal. Phase angles $< 30^\circ$ minimize atmospheric factors and maximize surface contrast.

4. Comparison to the infrared

We compare optical wavelength map in Fig. 3 to the previous infrared map in Fig. 4 to extend the region of spectral coverage. The optical map has less distinguished contrast within light and dark

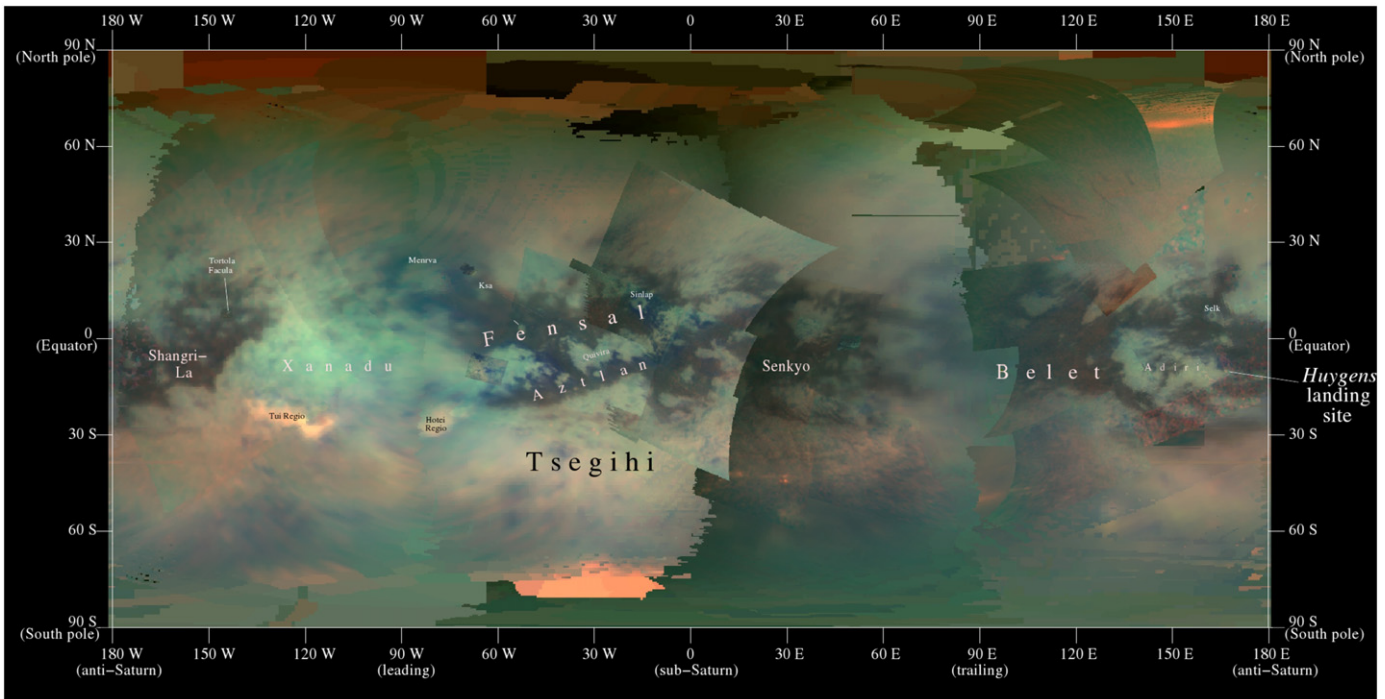


Fig. 4. This figure represents the work of Barnes et al. (2009) in mapping Titan using atmospheric windows in the infrared spectrum. The dark blue color on the optical wavelength map corresponds to the darkest green on the IR map. The bright orange color in the IR map represents the 5- μm active sites (bright orange features near the poles are clouds). Many differences can be seen comparing the infrared and visible maps. In particular Tsegihi shows up bright in the optical wavelengths, just as bright as Xanadu. While at 5 μm Tsegihi is actually brighter than Xanadu. At longer wavelengths Tsegihi is not as prominent and does not stand out from the rest of the area in the southern regions; but it does look different in the optical map. (For interpretation of the references to color in this figure legend, the reader is referred to the web version of this article.)

regions, whereas the infrared map described in Barnes et al. (2009) has many different distinguishable spectral variations within the light and dark regions. Since Titan appears gray within the optical windows, the single scattering albedo (the ratio of scattering efficiency to total extinction efficiency) must be a good approximation of the Bond albedo. The 5- μm bright areas, Tui Regio and Hotei Regio, for instance, do not appear distinguished from the rest of Xanadu.

The Selk and Sinlap craters are not resolved on the visible map. This is not due to the wavelength directly; a surface feature of this type should not depend on the wavelength in which it is observed unless the feature is covered in some optically sensitive material. The reason these craters do not appear is because of the resolution of the slit scanner on Cassini combined with the extra atmospheric scatter from working in the visual wavelengths. The VIMS-V scans at low resolution in order to compile a global view of Titan; however, a crater at most appearing in two pixels (See Table 1) will still fail to be resolved because of the high amount of atmospheric scattering, even though the ejecta blankets are apparent.

All of the light and dark albedo features, first described by Porco et al. (2005), are the focus of the discussion for surface composition. The next step is to do a systematic comparison of spectral types between the map in the visible (Figs. 3 and 6) to a well described IR map (Fig. 4) based on Barnes et al. (2007). The type of material each color and shade refers to is described in the aforementioned paper and will not be discussed here. A systematic comparison of each spectral signature in the IR methane windows to composition types can be found in McCord et al. (2008).

4.1. Equatorial zone

The equatorial zone bounded by 30° north and south of the equator is home to the greatest contrast on Titan's surface. VIMS-V can distinguish light and dark terrain, and the dark terrain is split into dark and light blue spectral types. The light colored (white)

terrain is slightly brighter across Xanadu and Tsegihi (Fig. 3) but is mostly uniform across Titan (Fig. 6).

4.1.1. Dark

The dark regime covers the majority of Titan's equatorial region and corresponds to the vast sand seas littering Titan's surface (Barnes et al., 2007; Soderblom et al., 2007). The placement of the dark areas agrees almost exactly with the dark brown spectral unit, giving us a good comparison standard. Although the resolution is coarser in the visible than in the IR, the boundaries between spectral types are sharper in the visible map in Fig. 6.

The eastern sections of the equatorial area in each map do not agree as well in the total surface features visible. Belet does not stand out as well in the visible map from being on a seam between flybys, thus making the emission angle higher, causing more haze and lower surface contrast. The section south of Adiri, however, is clearer in the visible. Just above the 30°S mark on the eastern end of the map, we can see the dark extend down into an open region not visible on the IR map. These new areas could be outlines of dune material.

4.1.2. Visible light blue

The light blue regime corresponds closely to the dark blue IR spectral unit but also covers additional area. In Fig. 6, the light blue serves as the midway between the white and dark areas. The light blue in the visible matches all of the dark blue areas in the IR map but also extends to some other areas, most notably: northern Shangri-La in the west, northeast Senkyo in the center, and around the outer fringes of Adiri in the east.

VIMS dark blue areas are thought to be dirty water ice (Rodriguez et al., 2006; Le Mouélic et al., 2008; Soderblom et al., 2007; Barnes et al., 2007) or organic compounds (Clark et al., 2010). Fig. 9 compares the water ice spectrum from Enceladus to a spectrum of the light blue (dark blue IR) spectral unit

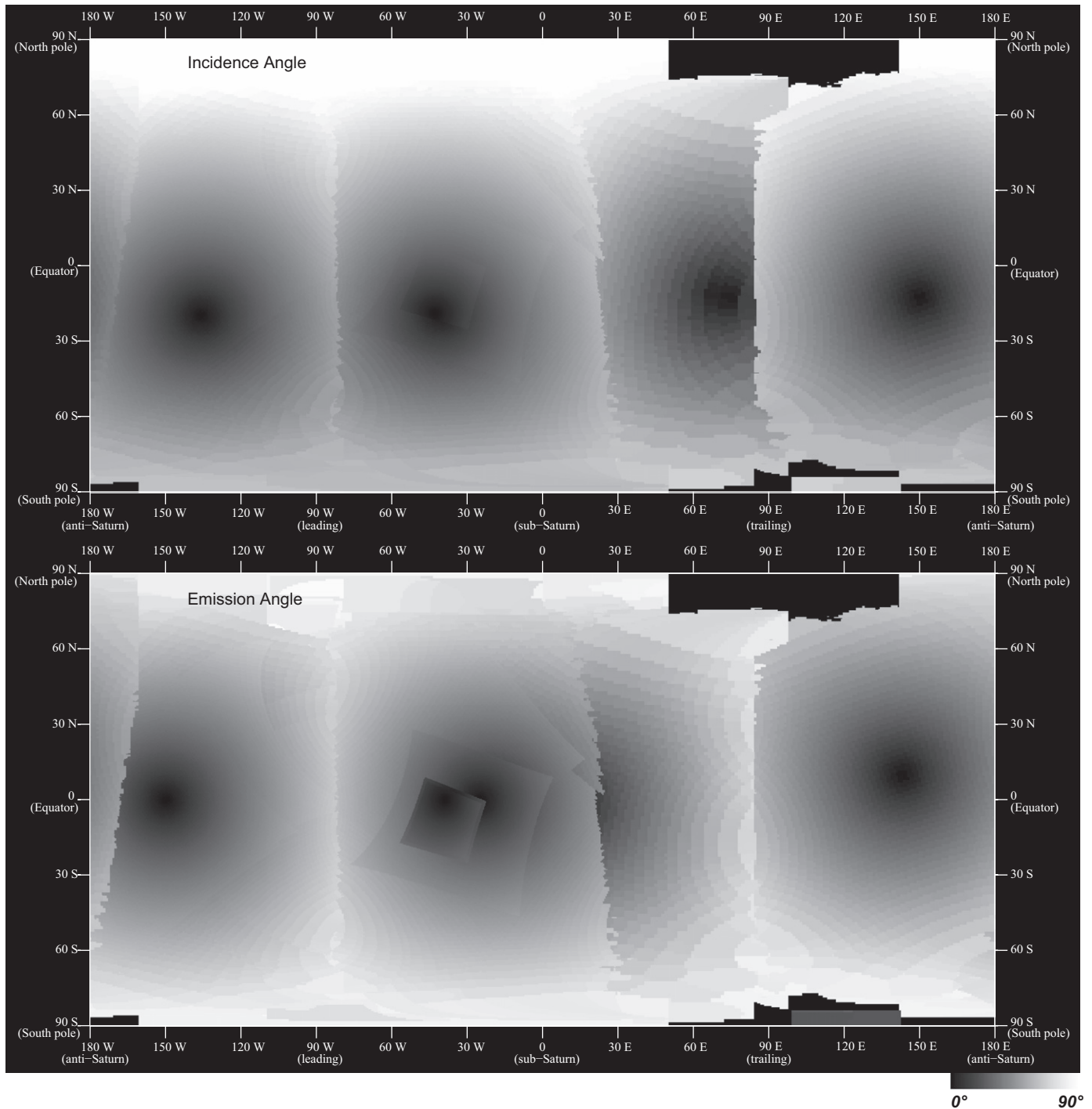


Fig. 5. The top map represents the incidence angle as it changes over each flyby. The bottom map represents the emission angle. The angle, in both cases, build up as we approach the center of a flyby, then starts to drops off. These maps identify the nadir points where the signal-to-noise ratio is the greatest in relation to the resolution in Figs. 3 and 6.

in northern Shangri-La, similar to Griffith et al. (2003). The overall reflectivity in Enceladus produces a much higher I/F since there is no atmosphere to contend with. However, the gray appearance and greater relative brightness of the light blue spectrum in the visible wavelengths is broadly consistent with water ice, but certainly does not rule out the many possible organic compounds.

4.1.3. Xanadu

While Xanadu stands out as a bright albedo feature in the IR, the difference between Xanadu and the rest of the bright terrain

in the visible maps is not as striking. Xanadu appears a little brighter in Fig. 3 than the rest of the bright terrain; also in Fig. 6, Xanadu is distinguished from its surroundings.

4.2. Mid latitude zone

The mid latitude zone on Titan extends from 30° to 60° north and south. On the IR map, these regions are fuzzy and have nothing of real note except for the brighter albedo feature Tsegihi. In the visible, there is a new area south of Shangri-La in the west not visible on the IR map. The 5 μm bright features on the IR map

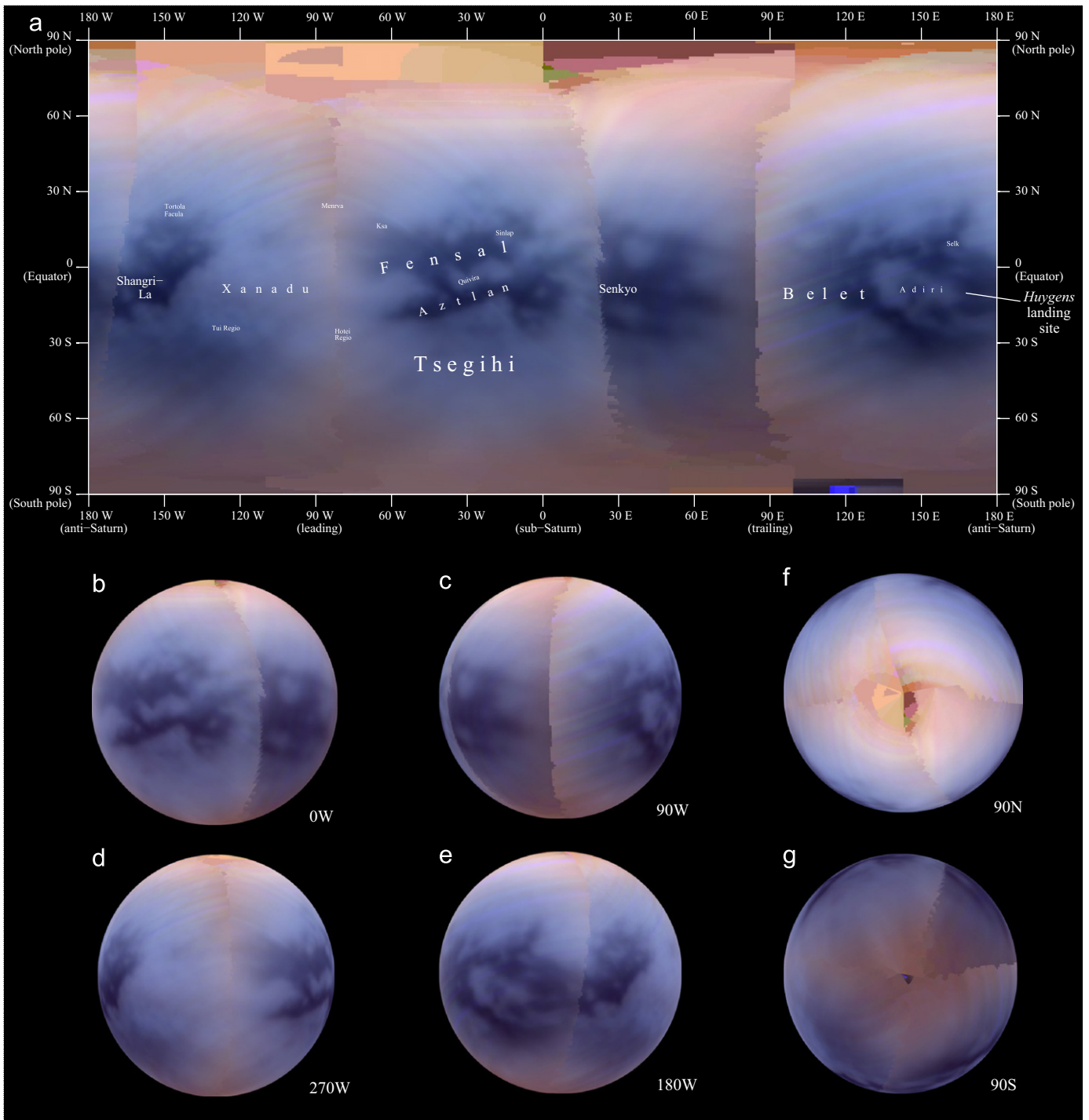


Fig. 6. This is a corrected global map of Titan, using the same color/wavelength scheme as Fig. 3, created using an algorithm to divide the haze out of the picture. In doing so, the surface features of Titan become more pronounced. Removing some of the haze also brings out the striping effects that are inherent to the VIMS-V system. When compared to Fig. 3, we can see new areas emerge, such as the section south of Shangri-La in the west.

are non-existent on the visible map; however, Tui Regio, south of Xanadu, can be described by its outline.

4.2.1. Tsegih

Tsegih is the second brightest large albedo feature in the IR. However, as seen in Fig. 3, Tsegih is the brightest albedo feature—even more so than Xanadu. This brightness of albedo may arise from the low phase angle of T9, the flyby comprising

90°W to roughly 20°E. In Fig. 6, with the haze removed, Tsegih appears, again, to be nothing of note and instead shows some splotches of light blue spectral types in the north and west areas corresponding to some light brown areas on the IR map.

4.2.2. Blue white

This section is lighter in color than the light blue in the equatorial region and exists south of Shangri-La. In the IR, this

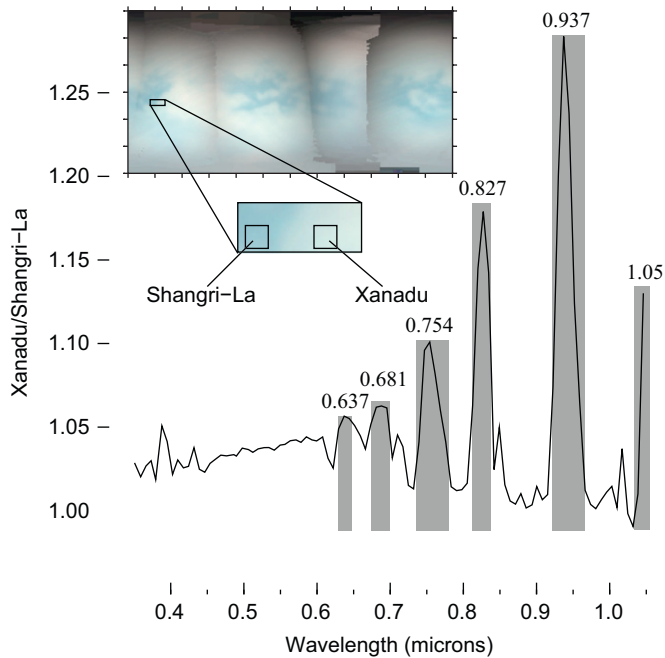


Fig. 7. A spectral ratio graph, created using the T8 flyby, depicting the detected flux from a bright area relative to that in a dark area. It represents the average value of Xanadu divided by Shangri-La versus wavelength in microns with optical wavelength windows labeled and the range of the windows boxed. At wavelengths with strong atmospheric absorption, the flux coming from Xanadu and that from Shangri-La are about the same, barring a small difference owing to different haze reflections resulting from view geometry. Within spectral windows, where there is little or no methane absorption, the much higher surface reflectivity of Xanadu results in higher ratios. The ratio for longer-wavelength windows is progressively higher than that for shorter-wavelength windows because the ratio is less affected by scattering off of haze particles. Windows exist at 0.637, 0.681, 0.754, 0.827, 0.937, and 1.05 μm .

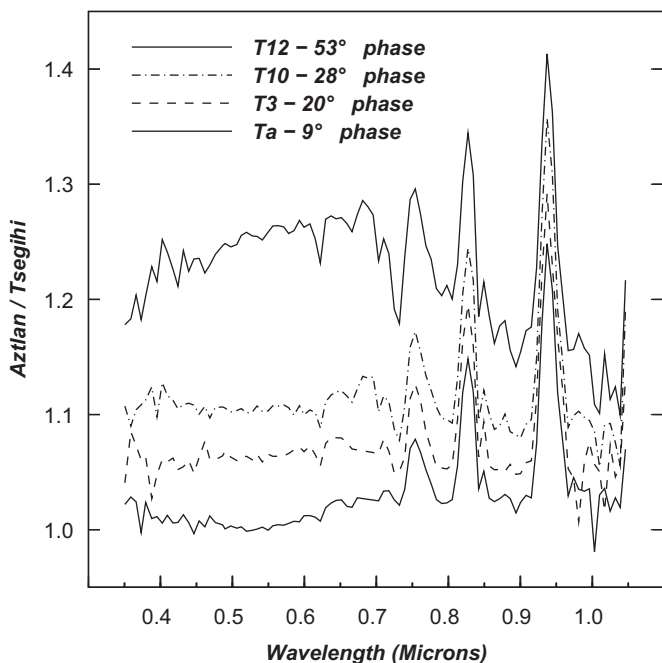


Fig. 8. The four lines above are spectral ratios from the same region as Fig. 7, T8 but at different phase angles, increasing from Ta to T12 by flyby number. The x-axis is wavelength in microns and the y-axis is albedo difference taken by dividing Xanadu by Shangri-La. As the phase angle goes up, the amount of striping noise in the spectrum goes up as is apparent by the rising and delinearization of the baseline. The height of each intensity peak remains unchanged above the baseline with increasing phase. The contribution from atmospheric scattering becomes more obvious in the plot of T12 in that lower wavelengths scatter more, raising the baseline.

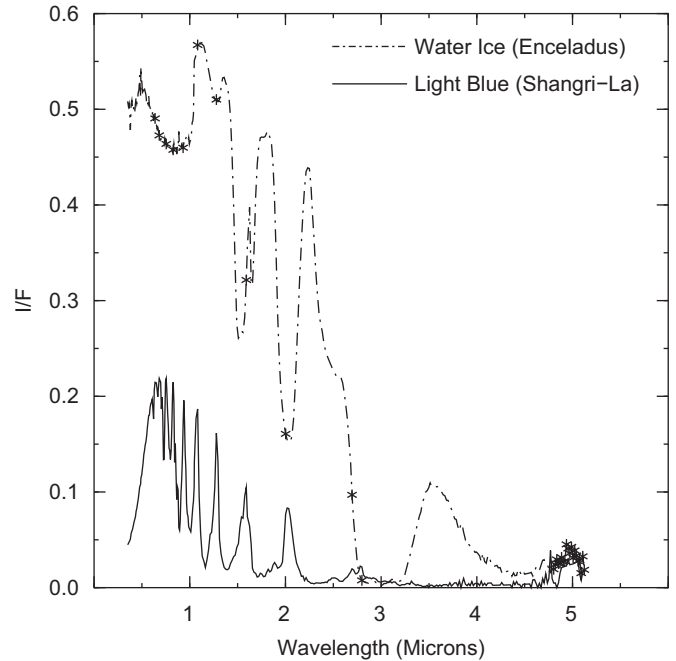


Fig. 9. A comparison between water ice (for reference) and the visible light blue spectral type taken from northern Shangri-La. The stars in the Enceladus line represent the atmospheric windows in both the visible and IR. The overall gray appearance and greater relative brightness compared to the IR in the visible wavelengths in the Titan spectrum is broadly consistent with water ice, and also with various organic materials. Inversions from minima to maxima in these graphs imply wavelengths where a signal may be transmitted without being absorbed.

section appears to be a group of 5- μm bright area with no real boundary. In the visible, however, we can make out a fringe between this blue white region, Tui Regio, and the surrounding area. This area in question is slightly larger than Shangri-La itself and has its southern boundary much more visible in Fig. 6.

4.2.3. White

The greatest area of Titan is comprised of white (Fig. 3) color corresponding to the equatorial bright spectral unit and many of the 5- μm bright areas of the IR map. This substrate covers the majority of Titan not occupied by the sand dunes.

5. Conclusion

The spectral albedo comparison of bright and dark surfaces on Titan confirm transmission peaks in the optical wavelengths. This gives targets to ground-based observers with Active Optics telescopes and allows for the possibility of resolving the surface of Titan using visible spectrum filters from Earth (Lemmon et al., 2002; Lorenz et al., 2003). This would allow more frequent data acquisition from a Moon so far away.

The visible spectrum mainly shows gray albedo changes for surface features on Titan. This serves as another constraint on surface composition to the IR maps published already. The main larger features on Titan are distinguishable at visible wavelengths but the smaller features and the 5- μm bright areas are not. We attributed this to either the lower spatial resolution (the spatial sampling does not change) of VIMS-V or to the inherent reflectivity of material on the surface that is apparent only in the IR, respectively. The improved surface contrast viewing Titan with

some haze removed, however, proves useful for seeing the extent to which certain surface features reach.

Our transmission spectrum in Fig. 7 is the major result from the visible wavelength observations for this paper. Knowing precisely where windows exist in the optical wavelengths can improve how spacecraft time is spent and what is targeted. If ground-based observers can resolve the surface of Titan, then those observations can be used to pick out targets for Cassini or any other spacecraft that may visit the Saturn system in the future.

The surface of Titan, scanned over all the visible VIMS channels, appears gray in each individual wavelength. All the photons Cassini receives back have been scattered to some extent but not absorbed by the atmosphere. We can make good use of the scattering albedo then as an approximation for the Bond albedo.

The IR wavelengths provide more spectral features for understanding the surface composition; but optical maps help to exclude surface materials not active in visible wavelengths, and as such provide a useful complement to longer-wavelength studies. This paper's intent is to report on wavelengths Cassini already scans, rather than arrive at specific constraints.

Acknowledgments

The work done here was made possible by NASA, ESA, and the VIMS team. The authors also acknowledge funding from Grant NNX09AP34G to J.W.B. from the NASA Outer Planets Research program. P. Cerroni, F. Capaccioni, A. Coradini, G. Filacchione and F. Tosi acknowledge the support of ASI Grant I/015/09/0.

References

- Barnes, J.W., Brown, R.H., Radebaugh, J., Buratti, B.J., Sotin, C., Le Mouélic, S., Rodriguez, S., Turtle, E.P., Perry, J., Clark, R., Baines, K.H., Nicholson, P.D., 2006. Cassini observations of flow-like features in western Tui Regio, Titan. *Geophysical Research Letters* 33 (August), L16204.
- Barnes, J.W., Brown, R.H., Soderblom, L., Buratti, B.J., Sotin, C., Rodriguez, S., Le Mouélic, S., Baines, K.H., Clark, R., Nicholson, P., 2007. Global-scale surface spectral variations on Titan seen from Cassini/VIMS. *Icarus* 186, 242–258.
- Barnes, J.W., Brown, R.H., Turtle, E.P., McEwen, A.S., Lorenz, R.D., Janssen, M., Schaller, E.L., Brown, M.E., Buratti, B.J., Sotin, C., Griffith, C., Clark, R., Perry, J., Fussner, S., Barbara, J., West, R., Elachi, C., Bouchez, A.H., Roe, H.G., Baines, K.H., Bellucci, G., Bibring, J.P., Capaccioni, F., Cerroni, P., Combes, M., Coradini, A., Cruikshank, D.P., Drossart, P., Formisano, V., Jaumann, R., Langevin, Y., Matson, D.L., McCord, T.B., Nicholson, P.D., Sicardy, B., 2005. A 5-micron-bright spot on Titan: evidence for surface diversity. *Science* 310, 92–95.
- Barnes, J.W., Soderblom, J.M., Brown, R.H., Buratti, B.J., Sotin, C., Baines, K.H., Clark, Jaumann, R., McCord, T.B., Nelson, R., Le Mouélic, S., Rodriguez, S., Griffith, C., Pentead, P., Tosi, F., Pitman, K.M., Soderblom, L., Stephan, K., Hayne, P., Vixie, G., Bibring, J., Bellucci, G., Capaccioni, F., Cerroni, P., Coradini, A., Cruikshank, D.P., Drossart, P., Formisano, V., Langevin, Y., Matson, D.L., Nicholson, P.D., Sicardy, B., 2009. VIMS spectral mapping observations of Titan during the Cassini prime mission. *Planetary and Space Science* 57, 1950–1962.
- Brown, R.H., Baines, K.H., Bellucci, G., Bibring, J.P., Buratti, B.J., Capaccioni, F., Cerroni, P., Clark, R.N., Coradini, A., Cruikshank, D.P., Drossart, P., Formisano, V., Jaumann, R., Langevin, Y., Matson, D.L., McCord, T.B., Mennella, V., Miller, E., Nelson, R.M., Nicholson, P.D., Sicardy, B., Sotin, C., 2004. The Cassini Visual and Infrared Mapping Spectrometer (VIMS) investigation. *Space Science Reviews* 115, 111–168.
- Capaccioni, F., Coradini, A., Cerroni, P., Amici, S., 1998. Imaging spectroscopy of Saturn and its satellites: VIMS-V onboard Cassini. *Planetary and Space Science* 46, 1263–1276.
- Clark, R.N., Curchin, J.M., Barnes, J.W., Jaumann, R., Soderblom, L., Cruikshank, D.P., Brown, R.H., Rodriguez, S., Lunine, J., Stephan, K., Hoefen, T.M., Le Mouélic, S., Sotin, C., Baines, K.H., Buratti, B.J., Nicholson, P.D., 2010. Detection and mapping of hydrocarbon deposits on Titan. *Journal of Geophysical Research (Planets)* 115 (October), E10005.
- Griffith, C.A., Owen, T., Geballe, T.R., Rayner, J., Rannou, P., 2003. Evidence for the exposure of water ice on Titan's surface. *Science* 300, 628–630.
- Griffith, C.A., Owen, T., Wagoner, R., 1991. Titan's surface and troposphere, investigated with ground-based, near-infrared observations. *Icarus* 93, 362–378.
- Karkoschka, E., 1994. Spectrophotometry of the Jovian planets and Titan at 300– to 1000-nm wavelength: the methane spectrum. *Icarus* 111 (September), 174–192.
- Le Mouélic, S., Paillou, P., Janssen, M.A., Barnes, J.W., Rodriguez, S., Sotin, C., Brown, R.H., Baines, K.H., Buratti, B.J., Clark, R.N., Crapeau, M., Encrenaz, P.J., Jaumann, R., Geudtner, D., Paganelli, F., Soderblom, L., Tobie, G., Wall, S., 2008. Mapping and interpretation of Sinlap crater on Titan using Cassini VIMS and RADAR data. *Journal of Geophysical Research (Planets)* 113 (April), E04003.
- Le Mouélic, S., Cornet, T., Rodriguez, S., Sotin, C., Barnes, J.W., Brown, R.H., Baines, K.H., Buratti, B.J., Clark, R.N., Nicholson, P.D., 2010. Empirical approaches to reduce the atmospheric component in VIMS surface images of Titan. AGU Fall Meeting Abstracts, December, C1546+.
- Lemmon, M.T., Smith, P.H., Lorenz, R.D., 2002. Methane abundance on Titan, measured by the space telescope imaging spectrograph. *Icarus* 160 (December), 375–385.
- Lockwood, G.W., Lutz, B.L., Thompson, D.T., Bus, E.S., 1986. The albedo of Titan. *Astrophysical Journal* 303 (April), 511–520.
- Lorenz, R.D., Dooley, J.M., West, J.D., Mitsugu, F., 2003. Backyard spectroscopy and photometry of Titan, Uranus, and Neptune. *Planetary and Space Science* 51 (February), 113–125.
- McCord, T.B., Hayne, P., Combe, J.P., Hansen, G.B., Barnes, J.W., Rodriguez, S., Le Mouélic, S., Baines, K.H., Buratti, B.J., Sotin, C., Nicholson, P., Jaumann, R., Nelson, R., 2008. The Cassini VIMS Team, 2008. Titan's surface: search for spectral diversity and composition using the Cassini VIMS investigation. *Icarus* 194, 212–242.
- McKay, C.P., Pollack, J.B., Courtin, R., 1989. The thermal structure of Titan's atmosphere. *Icarus* 80, 23–53.
- Neff, J.S., Humm, D.C., Bergstralh, J.T., Cochran, A.L., Cochran, W.D., Barker, E.S., Tull, R.G., 1984. Absolute spectrophotometry of Titan, Uranus, and Neptune 3500–10,500 Å. *Icarus* 60 (November), 221–235.
- Perry, J.E., McEwen, A.S., Fussner, S., Turtle, E.P., West, R.A., Porco, C.C., Knowles, B., Dawson, D.D., 2005. The Cassini ISS Team, 2005. Processing ISS images of Titan's surface. In: Mackwell, S., Stansbery, E. (Eds.), 36th Annual Lunar and Planetary Science Conference, pp. 2312–+.
- Porco, C.C., Baker, E., Barbara, J., Beurle, K., Brahic, A., Burns, J.A., Charnoz, S., Cooper, N., Dawson, D.D., Del Genio, A.D., Denk, T., Dones, L., Dyudina, U., Evans, M.W., Fussner, S., Giese, B., Grazier, K., Helfenstein, P., Ingersoll, A.P., Jacobson, R.A., Johnson, T.V., McEwen, A., Murray, C.D., Neukum, G., Owen, W.M., Perry, J., Roatsch, T., Spitale, J., Squyres, S., Thomas, P., Tiscareno, M., Turtle, E.P., Vasavada, A.R., Veverka, J., Wagner, R., West, R., 2005. Imaging of Titan from the Cassini spacecraft. *Nature* 434, 159–168.
- Porco, C.C., West, R.A., Squyres, S., McEwen, A., Thomas, P., Murray, C.D., Delgenio, A., Ingersoll, A.P., Johnson, T.V., Neukum, G., Veverka, J., Dones, L., Brahic, A., Burns, J.A., Haemmerle, V., Knowles, B., Dawson, D., Roatsch, T., Beurle, K., Owen, W., 2004. Cassini imaging science: instrument characteristics and anticipated scientific investigations at Saturn. *Space Science Reviews* 115, 363–497.
- Rannou, P., McKay, C.P., Lorenz, R.D., 2003. A model of Titan's haze of fractal aerosols constrained by multiple observations. *Planetary and Space Science* 51, 963–976.
- Richardson, J., Lorenz, R.D., McEwen, A., 2004. Titan's surface and rotation: new results from Voyager 1 images. *Icarus* 170, 113–124.
- Rodriguez, S., Le Mouélic, S., Sotin, C., Clénet, H., Clark, R.N., Buratti, B., Brown, R.H., McCord, T.B., Nicholson, P.D., Baines, K.H., 2006. The VIMS Science Team, 2006. Cassini/VIMS hyperspectral observations of the Huygens landing site on Titan. *Planetary and Space Science* 54, 1510–1523 (eprint0906.5476).
- Smith, P.H., Lemmon, M.T., Lorenz, R.D., Sromovsky, L.A., Caldwell, J.J., Allison, M.D., 1996. Titan's surface, revealed by HST imaging. *Icarus* 119, 336–349.
- Soderblom, L.A., Brown, R.H., Soderblom, J.M., Barnes, J.W., Kirk, R.L., Sotin, C., Jaumann, R., MacKinnon, D.J., Mackowski, D.W., Baines, K.H., Buratti, B.J., Clark, R.N., Nicholson, P.D., 2009. The geology of Hotei Regio, Titan: correlation of Cassini VIMS and RADAR. *Icarus* 204, 610–618.
- Soderblom, L.A., Kirk, R.L., Lunine, J.I., Anderson, J.A., Baines, K.H., Barnes, J.W., Barrett, J.M., Brown, R.H., Buratti, B.J., Clark, R.N., Cruikshank, D.P., Elachi, C., Janssen, M.A., Jaumann, R., Karkoschka, E., Mouélic, S.L., Lopes, R.M., Lorenz, R.D., McCord, T.B., Nicholson, P.D., Radebaugh, J., Rizk, B., Sotin, C., Stofan, E.R., Sucharski, T.L., Tomasko, M.G., Wall, S.D., 2007. Correlations between Cassini VIMS spectra and RADAR SAR images: implications for Titan's surface composition and the character of the Huygens probe landing site. *Planetary and Space Science* 55, 2025–2036.
- Stephan, K., Jaumann, R., Karkoschka, E., Barnes, J.W., Kirk, R., Tomasko, M.G., Turtle, E.P., Le Corre, L., Langshans, M., Le Mouélic, S., Lorenz, R., Perry, J., 2009. Mapping products of Titan's surface. In: Brown, R.H., Lebreton, J., Waite, J.H. (Eds.), Titan from Cassini-Huygens, pp. 489–510.
- Turtle, E.P., Perry, J.E., McEwen, A.S., Del Genio, A.D., Barbara, J., Dawson, D.D., West, R.A., Porco, C.C., 2009. Cassini imaging of Titan's high-latitude lakes, clouds, and south-polar surface changes. *Geophysical Research Letters* 36 (January), L02204.
- Turtle, E.P., Del Genio, A.D., Barbara, J.M., Perry, J.E., Schaller, E.L., McEwen, A.S., West, R.A., Ray, T.L., 2011. Seasonal changes in Titan's meteorology. *Geophysical Research Letters* 38 (February), L03203.